



# Characterization of 4.2-km-Deep Fractured Granodiorite Cores from Pohang Geothermal Reservoir, Korea

Saeha Kwon<sup>1</sup> · Linmao Xie<sup>1</sup> · Sehyeok Park<sup>1</sup> · Kwang-Il Kim<sup>1</sup> · Ki-Bok Min<sup>1</sup>  · Kwang Yeom Kim<sup>2</sup> · Li Zhuang<sup>2</sup> · Jaiwon Choi<sup>3</sup> · Hanna Kim<sup>4</sup> · Tae Jong Lee<sup>4</sup>

Received: 3 November 2017 / Accepted: 29 October 2018 / Published online: 2 November 2018  
© Springer-Verlag GmbH Austria, part of Springer Nature 2018

## Abstract

The rock core test is the most direct and reliable way to measure fundamental physical, hydraulic, and mechanical properties for underground reservoir characterization. A 10-cm diameter and 3.6-m-long granodiorite core was retrieved from a 4.2-km-deep geothermal well at the Pohang Enhanced Geothermal System (EGS) site in Korea. Numerous natural fractures were detected in the core and induced core disks were observed. We optimized the sample preparation with this limited core for various tests based on the scanned X-ray CT images that visualized all the fractures in the core. We measured the basic mechanical—the deformation and strength properties of intact rock—and thermal properties of intact samples. In particular, fracture deformation and strength properties were directly measured by conducting direct shear tests on pre-existing natural fractures. The seismic velocity and normal fracture stiffness were compared with the wireline logging and injection test measurements, respectively. The discrepancies between the in situ data and laboratory experiment are due to the stress dependency of properties. The measurements presented in this paper provide essential inputs for the EGS reservoir modelling and a dataset of properties for the fractured granite reservoir at a great depth from which few samples have been retrieved thus far.

**Keywords** Characterization of a fractured reservoir · Deep granite core · Natural fractures · Direct shear test

## 1 Introduction

In deep geological engineering applications, such as the production of shale gas, geo-sequestration of CO<sub>2</sub>, deep borehole disposal, and exploitation of deep geothermal energy, an essential first step is in determining the thermal, hydraulic, mechanical, and chemical properties of the reservoir. For instance, the fracture normal closure and shear dilation are critical components in an enhanced geothermal

system (EGS), which requires irreversible dilations of rock fractures by hydraulic stimulation to induce shear slip (Jung 2013). The feasibility of a successful EGS will be affected significantly by the range of variations in the geometry and mechanical properties of rock fractures. Furthermore, the compressive and tensile strength of the rocks are important inputs for evaluating the wellbore stability at great depths and for designing the hydraulic fracturing processes.

To provide a continuous record of the reservoir properties, well logs are extensively utilized for a reasonable time and cost. While well logging provides the frequency and orientations of intersecting fractures, it cannot estimate the mechanical properties of the fractures. Empirical equations may relate physical properties obtained from well loggings to strength parameters (e.g., Chang et al. 2006), but the estimated variations are too great to be used to analyze the wellbore stability. Rock cuttings can be used to determine the rock properties (Santarelli et al. 1998), but the small size and irregular shape of the cuttings forbid various rock mechanical tests in representative scale. Testing rock cores is the most direct way to determine the reservoir properties, but retrieving the cores from reservoirs at great depths is time

✉ Ki-Bok Min  
kbmin@snu.ac.kr

<sup>1</sup> Seoul National University, (08826) 1, Gwanak-ro, Gwanak-gu, Seoul, Republic of Korea

<sup>2</sup> Korea Institute of Civil Engineering and Building Technology, (10223) 283, Goyang-daero, Ilsanseo-gu, Goyang, Gyeonggi, Republic of Korea

<sup>3</sup> NEXGEO Inc, (05703) 16-15, Garakbon-Dong, Songpa-Gu, Seoul, Republic of Korea

<sup>4</sup> Korea Institute of Geoscience and Mineral Resources, (34132) 124, Gwahak-ro, Yuseong, Daejeon, Republic of Korea

consuming and financially costly (Rider 2002). Therefore, many geomechanical studies of the deep reservoir engineering and provision of hydraulic stimulation are being conducted with indirect or inferred geological data (e.g., Genter and Traineau 1992). The input parameters of reservoir geomechanical analysis and modelling were obtained by extrapolation from data on shallower formation (e.g., Valley and Evans 2007), empirical general data of a specific rock type (e.g., Shen 2008), data of other sites with similar reservoir conditions (e.g., Rutqvist et al. 2013), or indirect measurements derived from borehole loggings (Blöcher et al. 2010).

There are a few cases where the coring was performed at a great depth of crystalline rock formation to characterize each property. The Kola Superdeep Borehole in Russia (KSDB-3) is the deepest borehole in the world that has a final depth of 12,262 m. The direct measurement of physical and mechanical properties for the core samples recovered from the KSDB-3 borehole at a depth of 9904 m was reported (Trčková et al. 2002). The German Continental Drilling Program (KTB-HB) conducted coring below 4150 m and continued down to 9080 m at irregular intervals with a total recovery of 83.6 m (Berckheimer et al. 1997). In addition to being used to characterize the petrophysical and mechanical properties of the formation (Berckheimer et al. 1997; Chang and Haimson 2000), the cores were used to determine the stress state of the crust by core-based methods (Li and Schmitt 1998; Emmermann and Lauterjung 1997). For the Basel Deep Heat Mining project in Switzerland, a 10-m-long granite core was extracted near the bottom of the Basel-1 well at a depth of 4911 m (Valley and Evans 2015) to characterize the geomechanical and hydraulic properties of the target reservoir (Häring et al. 2008). Due to the

lack of eligible cores, the strength test was performed on a single sample (34 mm in diameter and 70 mm in length) using multi-stage confined compression tests (Valley and Evans 2015). Although there are four very deep wells at the Soultz EGS project in France, the core was extracted from the exploration well, EPS-1, between 1400 and 2300 m in the granite basement (Géraud et al. 2010).

To the authors' knowledge, comprehensive data on the mechanical and thermal properties of rock cores and rock fracture tests at depths beyond 4 km are sparse. Thus, more experiments must be performed to characterize deep reservoirs.

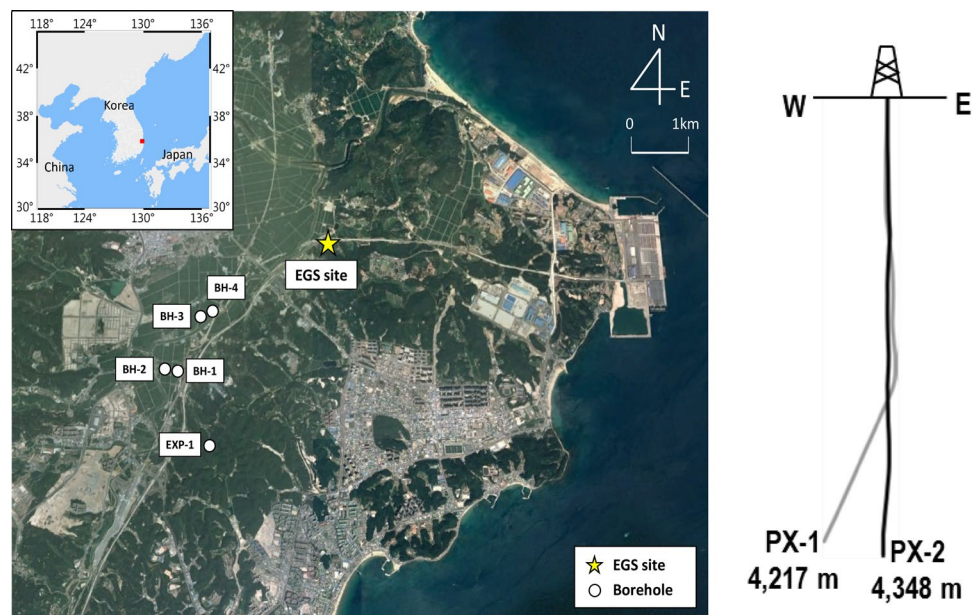
The purpose of this paper is to present the characterization of granodiorite cores and fractures retrieved from a depth of 4.2 km in the Pohang geothermal reservoir of South Korea. Comprehensive mechanical and thermal properties of deep rock cores are presented with the results of rock fracture tests for use as a well-archived dataset of fractured crystalline reservoir properties.

## 2 Geological Setting

### 2.1 Site Description

Pohang is located in the southeastern part of Korea and was selected as the pilot EGS project site due to the high geothermal gradient (Lee et al. 2010; Kim and Lee 2007). Five exploration wells were drilled beginning in 2003 to investigate the geological, geomechanical, and thermal conditions in the area (Fig. 1). Hydrofracturing and borehole observations were performed in exploration borehole EXP-1 to obtain in situ stress measurements (Kim et al. 2017). Rock

**Fig. 1** Location of Pohang EGS site and completed wells, which are five exploration wells within 5 km of the EGS site and two EGS wells with depths of 4217 and 4348 m (Park et al. 2018)



core samples were recovered at a depth of 1.1 km from borehole BH-1 and at a depth of 2.4 km from borehole BH-4 to perform the mechanical and thermal tests (Lee et al. 2015).

The geological structure of the Heunghae Basin, which underlies the Pohang EGS site, was deduced from geological and geophysical surveys and the drilling results of five wells (Fig. 2). The Heunghae Basin is covered with quaternary alluvium deposits that are underlain by thick tertiary sediments and sequential Cretaceous sediments. The granodiorite basement rock is present at depths below 2.2 km.

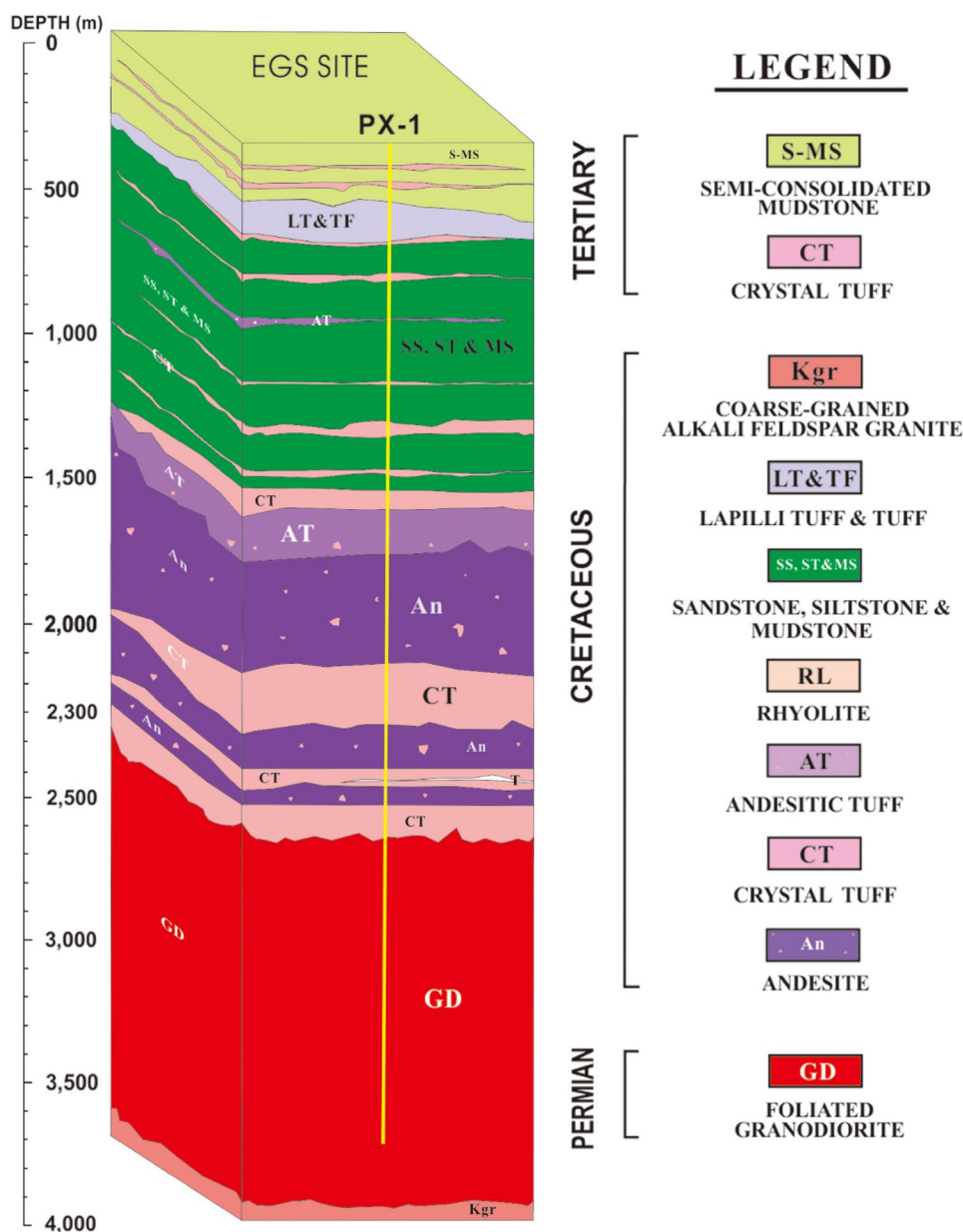
Two EGS wells, identified as PX-1 and PX-2, were drilled to depths of 4217 and 4348 m, respectively. Directional drilling of the PX-1 well was performed to ensure a suitable distance between the two wells in the reservoir. Five hydraulic

stimulation treatments were performed for PX-1 and PX-2 to map the artificial reservoir creation and to improve the hydraulic transmissivity (Park et al. 2018; Hoffman et al. 2018). Currently, the EGS project is suspended due to the earthquake (ML 5.4) on November 15, 2017 and investigation is under way on the casual linkage of the previous hydraulic stimulations and earthquake (KMA 2018; Grigoli et al. 2018).

### 2.2 Rock Core Description

An impregnated core bit was used for coring at depths starting at 4219 m in the PX-2 well. The granodiorite core was recovered from the PX-2 well, which was 3.6 m long and

**Fig. 2** Geological column deduced from cores and well logs of four exploration wells and the PX-1 well at the Pohang EGS site (modified from Lee et al. 2015). The PX-2 well is located 600 m from the PX-1



100 mm in diameter (Fig. 3). Retrieved cores contained numerous visible fractures, including pre-existing ones that were scattered over the core interval and induced core-disking fractures at the core bottom. Thirty-five fractures were identified, resulting in a fracture frequency of 9.7 fractures per meter. By counting core samples longer than 100 mm, the rock quality designation (RQD) of this core was determined to be 50.8% (Ulusay and Hudson 2007).

All the core samples were scanned by X-ray computed tomography (CT) to detect the natural and induced fractures not visible to the naked eye. A scanned image shows all of the fractures in a core sample (Fig. 4). Fracture mapping by X-ray CT scanning was used to optimize the arrangements of the core samples for various tests. Based on the core conditions, the core was divided into 11 sections, designated as S-I through S-XI (Fig. 3). The core-diskings were observed at the bottom section of the recovered cores. The shapes and thicknesses of the cored disks were measured from CT-scanned images (Fig. 4c). Furthermore, the disks were either flat or slightly saddle shaped with thicknesses ranging from 6.9 to 18.8 mm at a mean value of 12.3 mm.

Core plugs that are 25 mm in diameters were extracted from core section S-IV at 30° intervals (Fig. 3) for uniaxial compressive tests with acoustic emission (AE) monitoring to estimate the magnitudes of the stresses by the Kaiser effect (Lavrov 2003). Integrated in situ stress estimations in the Pohang geothermal reservoir were made using the results of the AE tests and core-disking analysis performed during characterization (Kim 2017).

The mineral composition of the core samples was analyzed by an X-ray diffractometer (XRD) and showed that the granodiorite core was composed mainly of 43.1% albite, 28.6% quartz, 13.7% microcline, and 10.1% muscovite. The microscopic distribution of the detected minerals was identified in the images from a polarization microscope (Fig. 5).

### 3 Characterization of Deep Rock Core and Fractures

A total of 20 mechanical (Tables 1, 2) and thermal (Table 3) parameters were determined. Although the available length of the core was limited due to numerous fractures, we were able to optimize the usage of the core to obtain various parameters in both intact rock and fractures due to CT imaging. The CT image led to the successful procurement of rock cores without unexpected breakage during sample preparation.

#### 3.1 Mechanical Tests on Rock Core

Compressive tests were conducted in a servo-controlled uniaxial and triaxial apparatus on cylindrical samples

to characterize the deformation and strength properties of intact rock. From the polarized microscope images (Fig. 5), the largest rock grain was about 1.2 mm. In addition, the diameter of the sample was 25 mm, which is 20 times greater than the grain size recommended by a standard method (Ulusay and Hudson 2007). Seven uniaxial compressive tests were conducted to obtain the complete stress–strain curves from which the uniaxial compressive strength (UCS), elastic modulus, and Poisson's ratio were derived. For seven tests, the measured mean value of UCS was 106.7 MPa with a standard deviation of 22.3 MPa. The measured mean values of elastic modulus and Poisson's ratio were 33.5 GPa and 0.21, respectively, for four tests.

Five triaxial compression tests were conducted to determine the cohesion and internal friction angle of the intact rock at confining stresses of 3, 5, 7, 10, and 15 MPa. According to the Mohr–Coulomb failure envelope obtained from all of the triaxial and uniaxial compression tests (Fig. 6), the estimated cohesion and internal friction angle of the rock were 15.2 MPa and 60.2°, respectively.

Two disc-shaped samples with diameters of 38 mm were taken from core section S-VII to determine the tensile strength using the Brazilian test. The Brazilian tensile strength of the rock was measured to be 9.2 MPa.

The P- and S-wave velocities were measured to be 4336 and 2676 m/s, respectively. The dynamic elastic modulus derived by the P- and S-wave velocities was 44.9 GPa, which was 34.0% larger than the static elastic modulus, as is often observed (Fjaer et al. 2008).

Wireline logging was performed in the PX-2 well and the properties under in situ conditions were indirectly derived using logging data. The porosity measured by wireline logging at the coring depth was 5.2%, which is 11 times greater than that from the laboratory tests, as the wireline logging results include the void volume of fractures.

The P- and S-wave velocities by wireline logging at the coring depth were 5920 and 3290 m/s, which are 36.4% and 22.7% higher values, respectively, than the ones obtained from the laboratory tests. The overburden stress at great depths can cause increased velocity of the seismic waves (Paillet and Cheng 1991). According to Troy Granite tests, which determine the relationship between stress and the velocity of seismic waves (Ellis 1987), P- and S-wave velocities increased drastically by 40% and 20%, respectively, compared with the velocities measured in the stress-free condition as the stress increased up to 40 MPa. When the stress was larger than 40 MPa, wave velocity change was minimal. It is known that the wave velocities decreased as the temperature increased, but the changes were minor for temperature increases up to 200 °C (Spencer and Nur 1976; Kern 1978). Thus, the discrepancy between the wave velocities obtained by well logging and by rock core measurements

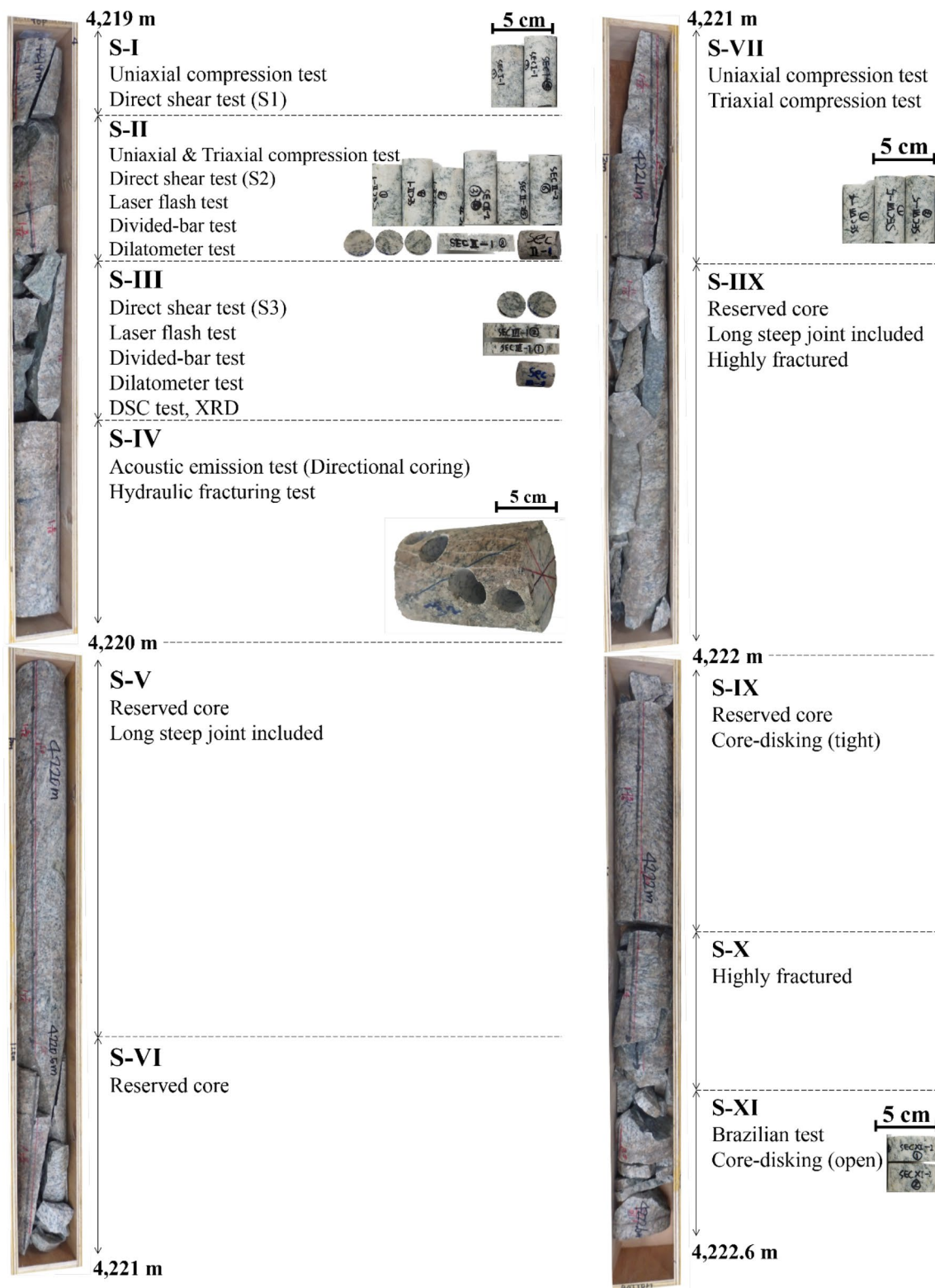
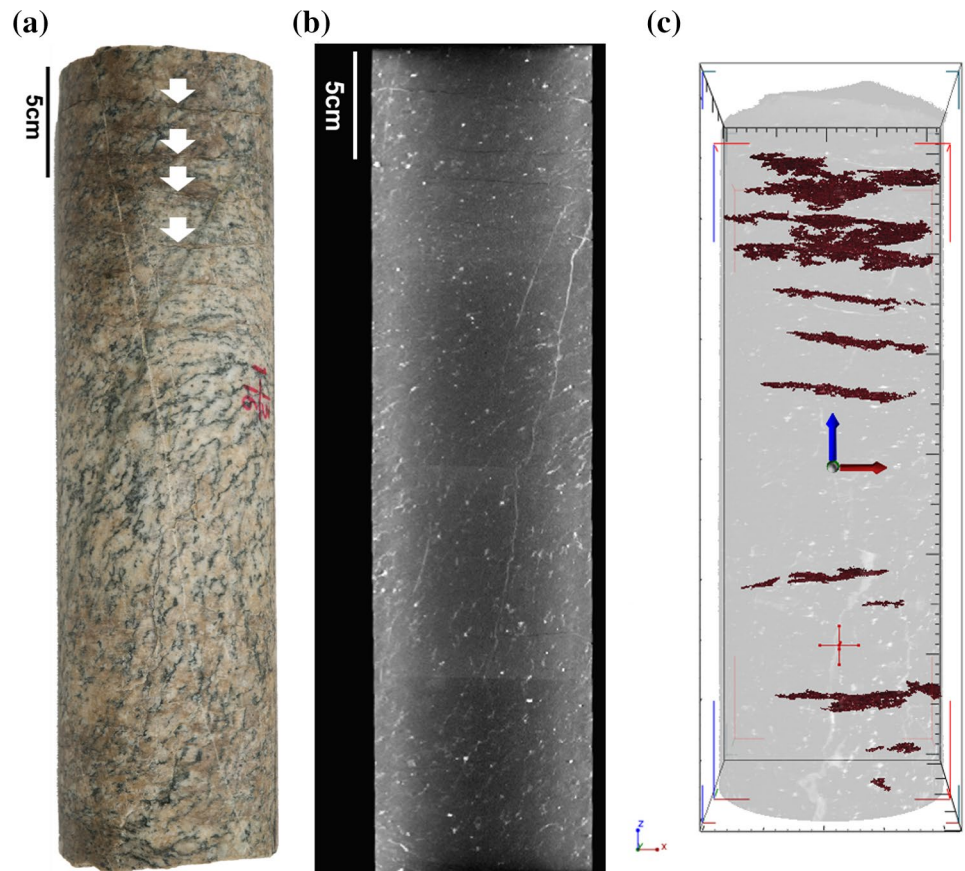


**Fig. 3** Photo of rock core samples obtained from the PX-2 well (3.6 m long and 100 mm in diameter) and detailed division of core samples for various tests

**Fig. 4** **a** Photograph of the rock core of section S-IX showing core-diskings in the upper part, **b** scanned image by X-ray CT technique, and **c** coordinates of fractures by X-ray CT technique



in this study was more likely due to the stress rather than the temperature.

### 3.2 Normal and Shear Behaviors of Natural Fractures

Fracture profiles are represented by the 3D coordinate data of the fracture surfaces, which allowed us to calculate the joint roughness coefficient (JRC) (Li and Zhang 2015; Diaz et al. 2017). For the seven fracture samples, the calculated JRC ranged from 8.7 to 16.0 at a mean value of 13.1. Interestingly, the anisotropy of the JRC ranges from 1.2 to 1.5 depending on the direction of the roughness measurement (Diaz et al. 2017).

Schmidt hammer tests were performed on five fracture samples that contained a sufficient natural fracture area. The rebound numbers were obtained by striking samples downward with a hammer. The lower half average of the test dataset was treated as the representative value (Ulusay 2015). The mean rebound number obtained for the weathered fracture was 50.8, which corresponds to the joint wall compressive strength (JCS) of 169.2 MPa.

Multi-stage direct shear tests were performed on selected natural fractures to simulate the shear behavior as well as to derive the fracture strength and deformability

properties (Muralha et al. 2014). Although recovered cores had numerous fractures (Fig. 3), fractured samples that were suitable for the direct shear test were limited, because the sizes of the blocks must be large enough to be representative of the cores and to mold the samples. Three fractured samples, referred to as S1, S2, and S3, were finally selected for the direct shear tests (Fig. 7a). Samples S1 and S3 included a highly dipped, natural fracture. Meanwhile, S2 had a sub-horizontal natural fracture. The sample blocks were molded to fit the shear box using Diastone, which has an elastic modulus of 8 GPa and UCS of 30 MPa (Lee and Song 2006).

Three-stage shear tests were conducted at servo-controlled constant normal stress conditions so that the displacement and stress could be recorded (Fig. 8). Samples S1 and S3 were broken during the second and third stages, respectively, and the associated data were discarded. In general, there was no clear peak shear strength observed during the experiment due to smooth fracture surfaces.

The coefficient of friction was 0.53, corresponding to a friction angle of the fracture of  $26.6^\circ$  as determined by fitting the normal stress-shear strength correlation. The coefficient of friction seems to be lower than the value typically used in practice (Byerlee 1978) because of smooth fracture surfaces and infilling material.

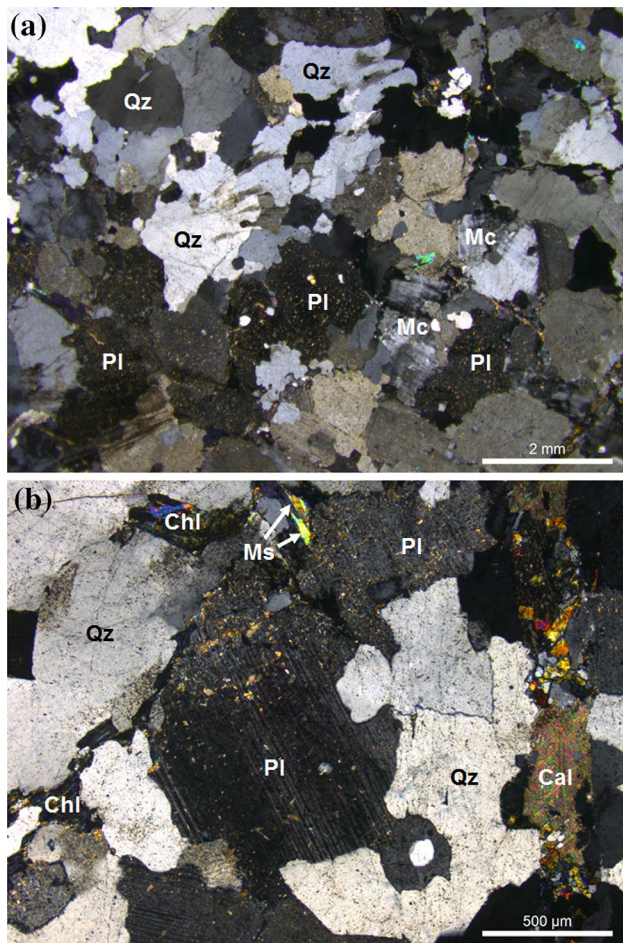


**Fig. 5** Polarization microscopic images with mineral descriptions for **a** crossed nicol at  $\times 12.5$  and **b** crossed nicol at  $\times 50$  (*Qz* quartz, *Pl* plagioclase, *Mc* microcline, *Ms* muscovite, *Chl* chlorite, *Cal* calcite)

Fracture normal stiffness was calculated during the application of normal stress by removing the portion of the normal deformation by Diastone and rock block. At stress levels of 1.6–4.8, 4.8–8.0, and 6.5–13.0 MPa, the fracture normal stiffness values were 7.9, 14.0, and 23.4 GPa/m, respectively,

which show an increase of normal stiffness with increasing applied normal stress. The normal stiffness obtained by direct measurement in the current study was compared with the one inferred from the hydraulic stimulation conducted in the Pohang PX-2 well in early 2016 (Park et al. 2018). The relationship between the equivalent aperture change of the single major fracture and the bottom hole pressure derived the normal stiffness of the reservoir system as ranging from 30.0 to 1695 GPa/m depending on the pressure level. This indicated reversible hydraulic jacking (Park et al. 2018). When high injection pressure was applied, which corresponded to low effective normal stress conditions, the normal stiffness derived from the field injection test was compatible with that determined by the fracture test in the current study. Yoo et al. (2018) employed the prescribed characterization results as the input parameters of the hydro-mechanical modelling of PX-2 hydraulic stimulation based on hydraulic jacking mechanism and the modelling successfully regenerated the field pressure-flow histories. The coherence of field monitoring, numerical modelling, and laboratory tests supports the notion that hydraulic jacking dominated during the hydraulic stimulation in the Pohang PX-2 well.

The dilation angle decreased as the normal stress increased in this study, which is consistent with other observations (Barton and Choubey 1977). For S3 (not shown here); however, an abnormally sharp increase of the dilation angle was detected during the second stage, which could have been caused by the partial failure of the rock block before the third stage.

The dilation angle obtained for normal stresses up to 8 MPa fit reasonably well with the empirical equation suggested by Barton and Choubey (1977) (Fig. 9). To evaluate the dilational behavior of rock fractures at a depth greater than 4 km, normal stresses of about 100 MPa had to be applied. Such tests will reveal the extent of the dilation angle that was reduced at the target depth of hydraulic stimulation for EGS. However, we were not able to apply such a high normal stress due to the limited capacity of the equipment.

**Table 1** Physical and mechanical properties derived from laboratory tests

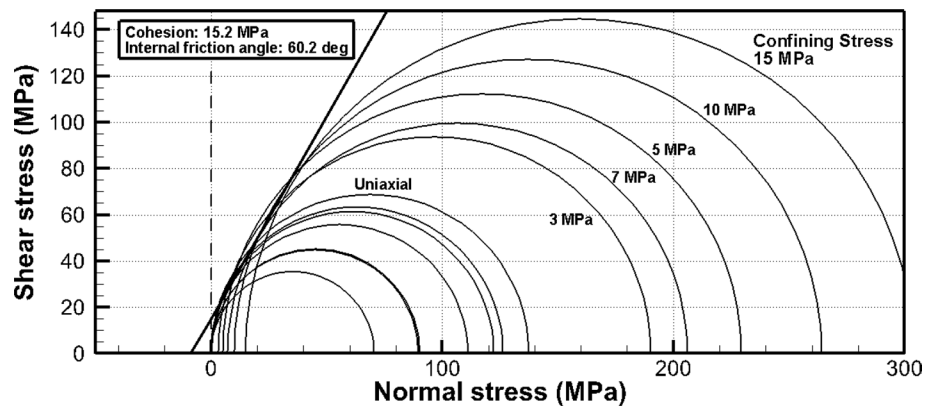
Property	Mean value	Standard deviation	No. of tests
Density (kg/m <sup>3</sup> )	2630	5	11
Porosity (%)	0.48	0.07	11
P-wave velocity (m/s)	4340	210	11
S-wave velocity (m/s)	2680	100	11
Elastic modulus (GPa)	33.5	6.8	4
Poisson's ratio	0.21	0.05	4
Uniaxial compressive strength (MPa)	106.7	22.3	7
Tensile strength (MPa)	9.2	0.4	2
Cohesion (MPa)	15.2	-	12
Internal friction angle (°)	60.2	-	12

**Table 2** Mechanical properties of fractures derived from laboratory tests

Property	Mean value	Standard deviation	No. of tests	Method
Joint wall compressive strength (MPa)	169.2	87.2	5	Schmidt hammer test (Barton and Choubey 1977; Aydin and Basu 2005)
Joint roughness coefficient	13.1	2.8	7	X-ray computed tomography (Li and Zhang 2015)
Friction angle of fracture (°)	26.6	0.5	2	Direct shear test (Ulusay 2015)
Normal stiffness of fracture (GPa/m)	7.9	–	1	1.6–4.8 MPa of normal stress
	14.0	–	1	4.8–8.0 MPa of normal stress
	23.4	–	1	6.5–13.0 MPa of normal stress
Shear stiffness of fracture (GPa/m)	3.2	1.7	3	
Dilation angle (°)	5.3	2.4	3	

**Table 3** Thermal properties derived from laboratory tests

Property	Mean value	Standard deviation	No. of tests	Method
Specific heat (kJ/kgK)	0.799	0.016	5	Laser flash method (ASTM E1461-13 2013b)
	0.804	0.044	5	Differential scanning calorimeter (ASTM E1269-11 2018)
Thermal conductivity (W/mK)	3.02	0.10	5	Laser flash method (ASTM E1461-13 2013b)
	2.98	0.30	3	Divided-bar method (Beardsmore and Cull 2001)
Thermal expansion coefficient (µm/m)	16.9	1.3	3	Dilatometer (ASTM D4535-13e2 2013a)

**Fig. 6** Mohr diagram consisting of Mohr stress circles for tri-axial and uniaxial compression tests and the derived Mohr–Coulomb failure envelope

Note that most of the available dilation data in the literature were obtained with normal stress levels less than 15 MPa. Therefore, more experiments are critically needed at higher levels of normal stress to predict more realistic dilational behavior at greater depths.

### 3.3 Thermal Tests on Rock Core

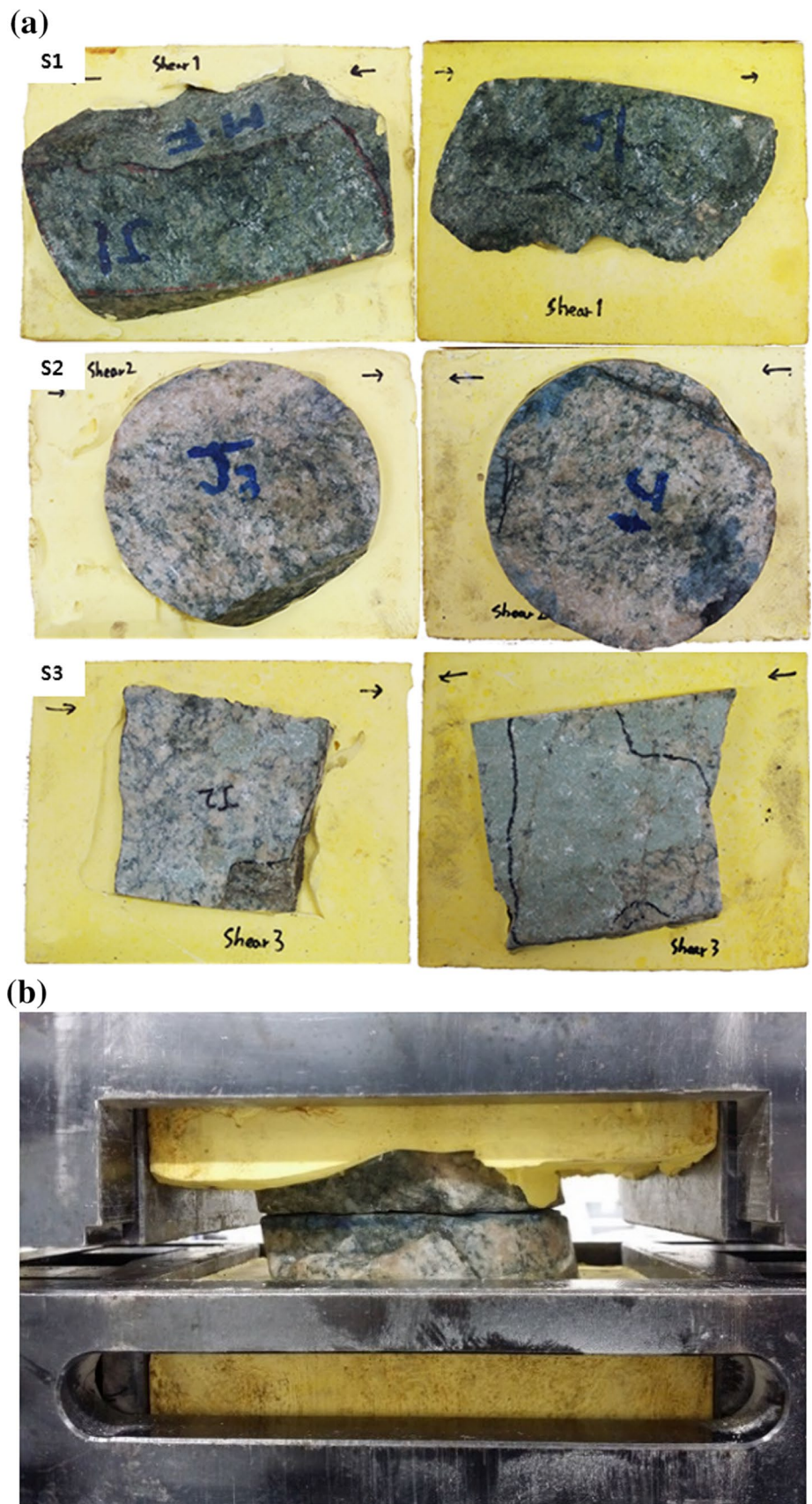
Thermal conductivity, specific heat capacity, and thermal expansion coefficient were measured for the recovered rock cores to characterize their thermal properties for use in evaluating the performance of the geothermal reservoir. The thermal expansion coefficients of the cylindrical samples

that had diameters of 20 mm were measured by a dilatometer (ASTM D4535-13e2 2013a). The expansion of samples was monitored as the temperature increased from 50 to 400 °C at a rate of 11 °C/min and the thermal expansion coefficient was derived from the recorded displacement–temperature curve. In addition, the mean thermal expansion coefficient of the three samples is  $1.7 \times 10^{-5}/\text{K}$ .

The specific heat was measured by the laser flash method (Zajas and Heiselberg 2013) and the differential scanning calorimeter (DSC) (ASTM E1269-11 2018). For the laser flash method, the specific heat was 0.799 kJ/kgK based on five disc-shaped samples with diameters of 25 mm and thicknesses of 3 mm. The tests were repeated three times



**Fig. 7** **a** Specimens molded for direct shear tests (the arrow represents the shearing direction during a direct shear test) and **b** molded sample placed in the shear box



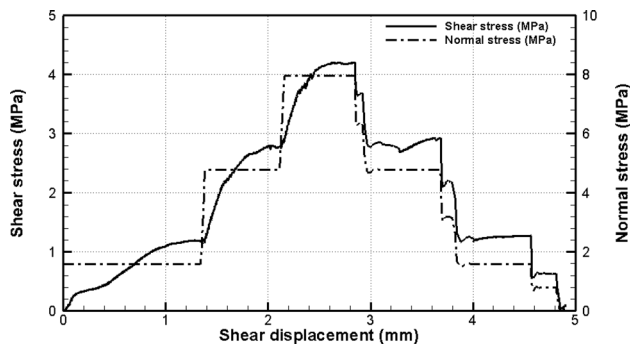


**Fig. 8** Direct shear test results for the S2 (normal and shear stress versus shear displacement). The three stages correspond to normal stress conditions at 1.6, 4.8, and 8.0 MPa

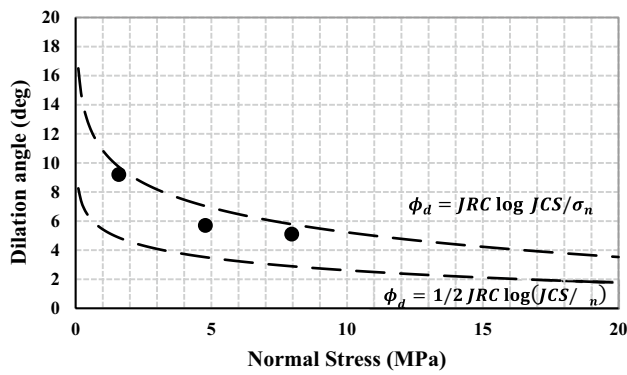


**Fig. 9** Trend lines of dilation angle with respect to normal stress based on an empirical equation developed by Barton and Choubey (1977) where  $\phi_d$  is the dilation angle, JRC is the joint roughness coefficient of fracture, JCS is the joint wall compressive strength, and  $\sigma_n$  is the normal stress applied on the surface of the fracture. The results of S2 (three dots) are within the trend lines

for each at room temperature. For the DSC method, the tests were performed on the disk-shaped samples that had diameters of 2 mm. Because the specimen was very small, special attention was paid to preparing more representative samples by choosing those that had mineral compositions similar to the ones in the entire rock core. The mean specific heat obtained for the five samples was 0.804 kJ/kgK at room temperature. The results of the DSC tests on small size disks were close to the results from the laser flash method used for the large samples.

The thermal conductivity was obtained by the laser flash method (ASTM E1461-13 2013b) and the divided-bar method (Beardsmore and Cull 2001). From the laser flash method, the mean thermal conductivity was calculated as 3.02 W/mK based on the thermal diffusivity and specific heat measurements. For the divided-bar method, disk-shaped samples with diameters of 54 mm were mounted between the lower and upper platens with heat sources at constant

temperatures of 10 °C and 40 °C, respectively. The tests lasted as long as 2000 s to guarantee that steady state was achieved during the test. The measured mean thermal conductivity for the three samples was 2.98 W/mK. In addition, the thermal conductivity was calculated indirectly from the mineralogical compositions determined by XRD analysis using the data compilation of Clauser and Huenges (1995). The arithmetic, geometric, and harmonic means of the mineral thermal conductivities were 3.54, 3.19, and 2.93 W/mK, respectively. The harmonic mean thermal conductivity of the minerals was the closest to the value obtained from direct measurements.

Birch and Clark (1940) reported a decreasing tendency for thermal conductivity when temperature increased. In the case of granite, the thermal conductivity at 0 °C was between 1.1 and 1.3 times the conductivity at 150 °C. Therefore, the thermal conductivity measured at room temperature is likely to slightly underestimate the thermal conductivity at a depth of 4.2 km where the temperature is 140 °C (Yoo et al. 2018).

## 4 Summary

Mechanical and thermal characterizations of rock and rock fractures are essential for borehole stability analyses as well as understanding the flow and transmissivity development when hydraulic stimulation is performed in a fractured reservoir. These properties are indispensable inputs for other deep geological applications such as deep borehole disposal of nuclear waste and geo-sequestration of CO<sub>2</sub>. We report on a set of mechanical and thermal properties for the granodiorite rock core and fractures retrieved from a depth of 4.2 km in the Pohang reservoir. The physical properties we measured included density, porosity, and P- and S-wave velocities. Uniaxial and triaxial compressive tests were conducted to determine the deformation and strength parameters of intact rock that include elastic modulus, Poisson's ratio, UCS, tensile strength, cohesion, and internal friction angle. Fracture properties, including JCS, JRC, basic friction angle, residual friction angle, normal stiffness, shear stiffness, and dilation angle, were determined for natural fractures in the core. Thermal properties, including thermal conductivity, heat capacity, and thermal expansion coefficient, were determined from measurements on the intact cores.

The determined mechanical and thermal properties of rock core and fractures were in the range typically expected in a granodiorite rock and a few notable observations were made:

- The stress-dependent normal stiffness of fractures matched reasonably well with observations made during in situ hydraulic stimulation at the deep fractured

reservoir, which demonstrates that the laboratory fracture test can help the interpretation of the hydraulic jacking mechanism.

- The dilation angles of the fracture determined from the laboratory tests with normal stress up to 8 MPa are within the range expected by the existing empirical formula. However, the experiment with much higher normal stress corresponding to deep reservoir is critically needed for more realistic evaluation of the dilational behavior of fractures.
- The friction coefficient of fracture was measured as 0.53, which is lower than the one typically used in practice because of the smooth fracture surface and infilling material.
- P- and S-wave velocities detected from well logging were 36.4% and 22.4% larger, respectively, than the ones estimated by laboratory tests, which is explained by the stress dependency of wave velocities.

**Acknowledgements** This research was supported by a Grant (No. 20133030000240) from the New and Renewable Energy Program of the Korea Institute of Energy Technology Evaluation and Planning, and funded by the Ministry of Trade, Industry and Energy of the Korean Government. Institute of Engineering Research at Seoul National University is acknowledged for the support on manuscript preparation. NexGeo Inc. provided support on the acquisition of the deep rock cores.

## References

- ASTM D4535-13e2 (2013a) Standard test methods for measurement of thermal expansion coefficient of rock using dilatometer. ASTM International, West Conshohocken
- ASTM E1461-13 (2013b) Standard test method for thermal diffusivity by the flash method, ASTM International, West Conshohocken
- ASTM E1269-11 (2018) Standard test method for determining specific heat capacity by differential scanning calorimetry. ASTM International, West Conshohocken
- Aydin A, Basu A (2005) The Schmidt hammer in rock material characterization. *Eng Geol* 81(1):1–14
- Barton N, Choubey V (1977) The shear strength of rock joints in theory and practice. *Rock Mech* 10(1–2):1–54
- Beardsmore G, Cull J (2001) *Crustal heat flow: a guide to measurement and modelling*. Cambridge University Press, Cambridge
- Berckhemer H, Rauen A, Winter H, Kern H, Kontny A, Lienert M, Nover G, Pohl J, Popp T, Schult A, Zinke J, Sofferl HC (1997) Petrophysical properties of the 9-km-deep crustal section at KTB. *J Geophys Res Solid Earth* 102(B8):18337–18361
- Birch F, Clark H (1940) The thermal conductivity of rocks and its dependence upon temperature and composition. *Am J Sci* 238(8):529–538
- Blöcher MG, Zimmermann G, Moeck I, Brandt W, Hassanzadegan A, Magri F (2010) 3D numerical modeling of hydrothermal processes during the lifetime of a deep geothermal reservoir. *Geofluids* 10(3):406–421
- Byerlee JD (1978) Friction of rocks. *Pure Appl Geophys* 116(4–5):615–626
- Chang C, Haimson B (2000) True triaxial strength and deformability of the German Continental Deep Drilling Program (KTB) deep hole amphibolite. *J Geophys Res Solid Earth* 105(B8):18999–19013
- Chang C, Zoback MD, Khaksar A (2006) Empirical relations between rock strength and physical properties in sedimentary rocks. *J Pet Sci Eng* 51:223–237
- Clauser C, Huenges E (1995) Thermal conductivity of rocks and minerals. In: Ahrens TJ (ed) *Rock physics and phase relations: a handbook of physical constants*. Am Geophys Union, Washington DC, pp 105–126
- Diaz M, Kim KY, Yeom S, Zhuang L, Park S, Min KB (2017) Surface roughness characterization of open and closed rock joints in deep cores using X-ray computed tomography. *Int J Rock Mech Min Sci* 98:10–19
- Ellis DV (1987) *Well logging for earth scientists*. Elsevier, Amsterdam
- Emmermann R, Lauterjung J (1997) The German continental deep drilling program KTB: overview and major results. *J Geophys Res Solid Earth* 102(B8):18179–18201
- Fjaer E, Holt RM, Horsrud P, Risnes R (2008) *Petroleum related rock mechanics*, 2nd edn. Elsevier, Amsterdam
- Genter A, Traineau H (1992) Borehole EPS-1, Alsace, France: preliminary geological results from granite core analyses for Hot Dry Rock research. *Sci Drill* 3:205–214
- Géraud Y, Rosener M, Surma F, Place J, Le Garzic É, Diraison M (2010) Physical properties of fault zones within a granite body: example of the Soultz-sous-Forêts geothermal site. *C R Geosci* 342(7–8):566–574
- Grigoli F, Cesca S, Rinaldi AP, Manconi A, López-Comino JA, Clinton JF, Westaway R, Cauzzi C, Dahm T (2018) The November 2017 Mw 5.5 Pohang earthquake: a possible case of induced seismicity in South Korea. *Science* 360(6392):1003–1006
- Häring MO, Schanz U, Ladner F, Dyer BC (2008) Characterisation of the Basel 1 enhanced geothermal system. *Geothermics* 37(5):469–495
- Hofmann H, Zimmermann G, Farkas M, Huenges E, Zang A, Leonhardt M, Kwiatek G, Martinez-Garzon P, Bohnhoff M, Min KB, Fokker P, Westaway R, Bethmann F, Meier P, Yoon K, Choi J, Lee TJ, Kim KY (2018) First field application of cyclic soft stimulation at the Pohang Enhanced Geothermal System site in Korea. *Geophys J Int* (**under review**)
- Jung R (2013) EGS—goodbye or back to the future. In: *International conference for effective and sustainable hydraulic fracturing*, Brisbane, pp 95–121
- Kern H (1978) The effect of high temperature and high confining pressure on compressional wave velocities in quartz-bearing and quartz-free igneous and metamorphic rocks. *Tectonophysics* 44(1):185–203
- Kim H (2017) *Integrated estimation of in-situ rock stress at Pohang geothermal reservoir in Korea*. PhD Dissertation, Seoul National University
- Kim HC, Lee Y (2007) Heat flow in the Republic of Korea. *J Geophys Res* 112:B05413
- Kim H, Xie L, Min KB, Bae S, Stephansson O (2017) Integrated in-situ stress estimation by hydraulic fracturing, borehole observation and numerical analysis at the EXP-1 borehole in Pohang, Korea. *Rock Mech Rock Eng*. <https://doi.org/10.1007/s00503-017-1284-1>
- Korea Meteorological Administration (2018) Earthquake information. [http://www.kma.go.kr/eng/weather/current\\_state/information.jsp](http://www.kma.go.kr/eng/weather/current_state/information.jsp). Accessed 26 Mar 2018
- Lavrov A (2003) The Kaiser effect in rocks: principles and stress estimation techniques. *Int J Rock Mech Min Sci* 40(2):151–171
- Lee SW, Song JJ (2006) A study on the change of uniaxial compressive strength and Young's modulus according to the specimen size of intact material. *Tunn Tech* 8(3):205–207 (**Korean**)
- Lee Y, Park S, Kim J, Kim HC, Koo MH (2010) Geothermal resource assessment in Korea. *Renew Sustain Energy Rev* 14(8):2392–2400

- Lee TJ, Song Y, Park DW, Jeon J, Yoon WS (2015) Three dimensional geological model of Pohang EGS Pilot Site, Korea. In: World Geothermal Congress 2015, Melbourne (**paper 31025**)
- Li Y, Schmitt DR (1998) Drilling-induced core fractures and in situ stress. *J Geophys Res Solid Earth* 103(B3):5225–5239
- Li Y, Zhang Y (2015) Quantitative estimation of joint roughness coefficient using statistical parameters. *Int J Rock Mech Min Sci* 77:25–35
- Muralha J, Grasselli G, Tatone B, Blumel M, Chryssanthakis P, Yujing J (2014) ISRM suggested method for laboratory determination of the shear strength of rock joints: revised version. *Rock Mech Rock Eng* 47:291–302
- Paillet FL, Cheng CH (1991) *Acoustic waves in boreholes*. CRC Press, Boca Raton
- Park S, Kim KI, Xie L, Kwon S, Yoo H, Min KB, Choi J, Yoon WS, Yoon K, Song Y, Lee TJ, Kim KY, Zimmermann G, Guinot F, Meier P (2018) The first hydraulic stimulations in a fractured geothermal reservoir in Pohang, South Korea—part I. Observations and analysis (**manuscript**)
- Rider M (2002) The geological interpretation of well logs. Rider-French Consult Ltd., Scotland
- Rutqvist J, Rinaldi AP, Cappa F, Moridis GJ (2013) Modeling of fault reactivation and induced seismicity during hydraulic fracturing of shale-gas reservoirs. *J Pet Sci Eng* 107:31–44
- Santarelli FJ, Marsala AF, Brignoli M, Rossi E, Bona N (1998) Formation evaluation from logging on cuttings. *SPE Reserv Eval Eng* 1(3):238–244
- Shen B (2008) Borehole breakouts and in situ stresses. In: *Proceedings of the First Southern Hemisphere International Rock Mechanics Symposium*, Australian Centre for Geomechanics, Perth, pp 407–418
- Spencer JW, Nur AM (1976) The effects of pressure, temperature, and pore water on velocities in Westerly granite. *J Geophys Res* 81(5):899–904
- Trčková J, Živor R, Píkrýl R (2002) Physical and mechanical properties of selected amphibolite core samples from the Kola Super-deep Borehole KSDB-3. *Terra Nova* 14(5):379–387
- Ulusay R (2015) *The ISRM suggested methods for rock characterization, testing and monitoring: 2007–2014*. Springer, Cham
- Ulusay R, Hudson JA (2007) *The complete ISRM suggested methods for rock characterization, testing and monitoring: 1974–2006*. ISRM Turkish National Group, Ankara
- Valley B, Evans KF (2007) Stress state at Soultz-sous-Forêts to 5 km depth from wellbore failure and hydraulic observations. In: *Proceedings, 32nd workshop on geothermal reservoir engineering*, Stanford, pp 17481–17469
- Valley B, Evans KF (2015) Estimation of the stress magnitude in Basel enhanced geothermal system. In: *World Geothermal Congress 2015, Melbourne*, pp 19–25
- Yoo H, Park S, Xie L, Min KB, Rutqvist J, Rinaldi AP (2018) The first hydraulic stimulations in a fractured geothermal reservoir in Pohang, South Korea—Part II. Numerical Modeling (**manuscript**)
- Zajas J, Heiselberg P (2013) Measurements of thermal diffusivity, specific heat capacity and thermal conductivity with LFA 447 apparatus. DCE technical report 144. Aalborg University, Denmark

**Publisher's Note** Springer Nature remains neutral with regard to jurisdictional claims in published maps and institutional affiliations.